Icarus 245 (2015) 273–281

Contents lists available at ScienceDirect

Icarus

journal homepage: www.elsevier.com/locate/icarus

Fresh clouds: A parameterized updraft method for calculating cloud densities in one-dimensional models

Michael H. Wong [a,b,*], Sushil K. Atreya [a], William R. Kuhn [a], Paul N. Romani [c], Kristen M. Mihalka [a]

[a] Department of Atmospheric, Oceanic, and Space Science, University of Michigan, Ann Arbor, MI 48109-2143, USA
[b] Astronomy Department, University of California, Berkeley, CA 97420-3411, USA
[c] NASA Goddard Space Flight Center, Greenbelt, MD 20771, USA

ARTICLE INFO

Article history:
Received 15 May 2014
Revised 20 September 2014
Accepted 23 September 2014
Available online 2 October 2014

Keywords:
Atmospheres, structure
Atmospheres, chemistry
Meteorology
Jupiter, atmosphere
Extra-solar planets

ABSTRACT

Models of cloud condensation under thermodynamic equilibrium in planetary atmospheres are useful for several reasons. These equilibrium cloud condensation models (ECCMs) calculate the wet adiabatic lapse rate, determine saturation-limited mixing ratios of condensing species, calculate the stabilizing effect of latent heat release and molecular weight stratification, and locate cloud base levels. Many ECCMs trace their heritage to Lewis (Lewis, J.S. [1969]. Icarus 10, 365–378) and Weidenschilling and Lewis (Weidenschilling, S.J., Lewis, J.S. [1973]. Icarus 20, 465–476). Calculation of atmospheric structure and gas mixing ratios are correct in these models.

We resolve errors affecting the cloud density calculation in these models by first calculating a cloud density rate: the change in cloud density with updraft length scale. The updraft length scale parameterizes the strength of the cloud-forming updraft, and converts the cloud density rate from the ECCM into cloud density. The method is validated by comparison with terrestrial cloud data.

Our parameterized updraft method gives a first-order prediction of cloud densities in a "fresh" cloud, where condensation is the dominant microphysical process. Older evolved clouds may be better approximated by another 1-D method, the diffusive–precipitative Ackerman and Marley (Ackerman, A.S., Marley, M.S. [2001]. Astrophys. J. 556, 872–884) model, which represents a steady-state equilibrium between precipitation and condensation of vapor delivered by turbulent diffusion.

We re-evaluate observed cloud densities in the Galileo Probe entry site (Ragent, B. et al. [1998]. J. Geophys. Res. 103, 22891–22910), and show that the upper and lower observed clouds at ~0.5 and ~3 bars are consistent with weak (cirrus-like) updrafts under conditions of saturated ammonia and water vapor, respectively. The densest observed cloud, near 1.3 bar, requires unexpectedly strong updraft conditions, or higher cloud density rates. The cloud density rate in this layer may be augmented by a composition with non-NH_4SH components (possibly including adsorbed NH_3).

1. Introduction

One-dimensional equilibrium cloud condensation models, or ECCMs, are simple first-order descriptions of clouds and their compositions in planetary atmospheres. Lewis, (1969; hereafter L69) pioneered this type of model for Jupiter, describing clouds composed of ammonia ice, ammonium hydrosulfide or other compounds formed by NH_3 and H_2S, water ice, and a liquid water solution cloud including dissolved NH_3 and H_2S. Weidenschilling and Lewis, (1973; hereafter WL73) updated the model to include condensation of CH_4 and Ar, potentially relevant to the cold ice giants Uranus and Neptune.

Conceptually, ECCMs are described by the ascent of a parcel of air under hydrostatic, wet adiabatic conditions (Fig. 1). Initial conditions are set at a deep tropospheric level where the relative humidity of all volatile components is less than 100% (subsaturated conditions). The parcel moves upward at each model step, with temperature and pressure controlled by hydrostatic equilibrium and the ideal gas law. This yields the dry adiabatic lapse rate at deep levels where nothing condenses. Once the model reaches saturation in one of its volatile components, latent heat effects are included to produce the moist adiabatic lapse rate, which changes with height depending on the abundances of volatile gases remaining at each level. A key principle of these models is that the

* Corresponding author at: Astronomy Department, University of California, Berkeley, CA 97420-3411, USA.

http://dx.doi.org/10.1016/j.icarus.2014.09.042
0019-1035/

condensed material remains at the condensation level; the ascending parcel retains only gaseous volatiles.

The WL73 scheme has been widely cited[1] and extensively used in development of more complex models, in interpretation of planetary data, and in predicting atmospheric conditions. A new 1-D model for determining cloud densities, whose major advance was the inclusion of turbulent diffusion, was introduced by Ackerman and Marley, (2001; hereafter AM01). Condensate density in AM01 was based on the L69 scheme.[1]

Despite more than 40 years of elapsed time since ECCMs were developed, they remain highly relevant today. The drawback to these models is that they do not include complex dynamics (3-D circulation controlling cloud formation) or microphysics (time-dependent evolution of particle creation, evolution, and loss). However, these models are computationally cheap, and they efficiently perform a variety of tasks relevant on their own, or as inputs to more complex models. Specifically, ECCMs are ideal for the following calculations:

- Determine the wet/dry adiabatic lapse rates in a planetary atmosphere as a function of height, composition, and temperature. This also gives atmospheric static stability.
- Determine the cloud base lifting condensation level (LCL), for any conceivable condensing species.
- Determine the composition of condensed clouds present in a planetary atmosphere, as a function of temperature and gas composition (requires that the proper thermodynamic data are included for all potential condensates).

Since the original models (L69 and WL73), some concern has been present about the fidelity of the cloud densities output by the models. Weidenschilling and Lewis (1973) noted that output cloud densities in L69 depended on the step size used in the numerical model, an unphysical effect. In WL73 itself, the authors stated that an authentic physical interpretation of their modeled cloud densities might be evasive. Lewis, (1995, p. 157) suggested that WL73 cloud densities are overestimated, but that the shape of the vertical profile accurately gives the relative cloud mass as a function of height. Recently, it was brought to our attention that the cloud densities calculated by WL73 actually violate conservation of mass, a serious flaw in the algorithm. There is thus a need to revise the cloud density algorithm within these models.

An improvement to the cloud density calculation is described below, in which the ECCM directly calculates a "cloud density rate" (with respect to height), rather than a cloud density. A cloud density rate essentially gives the rate of condensate formation, depending on the updraft length scale, L. This length scale can be written as a product of the updraft velocity and time scales: $w_*\tau_d$. The method provides a first-order model of cloud formation via condensation, as a function of updraft strength. We validate the approach by successfully comparing it to cloud densities and updraft parameters for terrestrial cirrus and cumulus clouds, and then apply the method to the Galileo Probe entry site, where cloud densities were measured in situ by a nephelometer (Ragent et al., 1998).

2. Condensate density algorithms

2.1. Weidenschilling and Lewis (1973)

Cloud density in WL73 was derived from the derivative of column mass density, which in a hydrostatic isothermal atmosphere can be given by the handy rules of thumb:

[1] A search of the publications database in NASA's Astrophysics Data System yields some 100 peer reviewed citations to WL73, and over 200 citations to AM01.

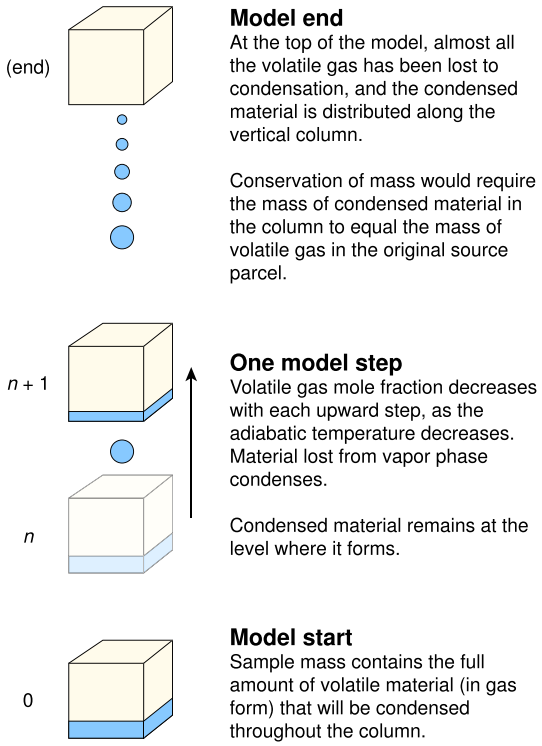

Fig. 1. Overview of the equilibrium cloud condensation model's treatment of volatile material.

$$\sigma(J) = \int_J^\infty \rho(z)dz = \int_J^\infty \rho_0 e^{-z/H}\,dz = -\rho_0 H e^{-z/H}\big|_J^\infty = \rho(J)H = P(J)/g, \quad (1)$$

where symbols are given in Table 1 and the last line makes use of the ideal gas law and the definition of scale height, $H = k_B T/\bar{\mu} m_H g$.

For a single volatile component x, WL73 give the gas column density as $m_x\sigma$. In the method used in WL73, the cloud density D_x at a given layer is then given by the differential with respect to altitude of the column density, approximated by the difference in mass fraction divided by the altitude step. Eq. (19) of WL73 gives the cloud density for species x as

$$D_x = -\frac{dm_x}{dz}\sigma = -\frac{\mu_x}{\bar{\mu}}\frac{dX_x}{dz}\rho H \approx \frac{\mu_x}{\bar{\mu}}\frac{X_x(I) - X_x(J)}{\Delta}\rho H. \quad (2)$$

Within the ascending parcel paradigm of the ECCM as described in Fig. 1, the condensate densities in WL73 violate conservation of mass. The mass of condensate within a column above a given level, integrated to infinite altitude, should not exceed the mass of condensable vapor within the original source parcel before condensation.

To evaluate this criterion, consider the nominal Jupiter cloud model presented in Fig. 3 of WL73. At the base of the water cloud, the condensate density is 2.4×10^{-5} g cm^{-3}, the pressure is 7.1 bar, and the temperature is 277 K. Applying the ideal gas law and using the water mole fraction of 1.05×10^{-3} from their Table 1, the water vapor mass density near the cloud base is 5.9×10^{-6} g cm^{-3}. The density in this single layer already violates conservation of mass, because the condensate density is four times greater than the vapor density: one cannot squeeze 4 kg of water from a sponge whose original wet mass is 1 kg. The condensate column density above 7.1 bar—which is the total condensed matter originally derived from the ascending parcel—is a mass per unit area that is several orders of magnitude greater than the mass of condensable vapor in the original parcel of unit volume.

Table 1
Math symbols, units, and non-standard acronyms used in the text. Many symbols are common to WL73 or AM01, and described more fully there.

Symbol	Definition	Symbol	Definition
D_x	Cloud density (g cm^{-3})	ρ	Atmospheric gas density (g cm^{-3})
$f_{\rm rain}$	Precipitation efficiency (see AM01)	R_x	Cloud density rate (g cm^{-3} cm^{-1})
g	Effective gravitational acceleration, 22.66 cm s^{-2} at the Galileo Probe site	σ	Atmospheric column density; written M_J in WL73 (g cm^{-2})
H	Atmospheric scale height (cm)	T	Temperature (K)
I,J	Indices for adjacent model layers (layer J is above layer I)	τ_d	Updraft timescale (s)
K	Eddy diffusion coefficient (cm^{-2} s^{-1})	w_*	Updraft velocity or convective velocity scale (cm s^{-1})
$k_{\rm B}$	Boltzmann constant, 1.38×10^{-16} erg K^{-1}	x	Subscript, indicates variable refers to a specific volatile species x
L	Convective length scale (cm)	X_x	Species x mole fraction, $n_x/\bar{n}$
m_x	Mass fraction of species x (g/g)	z	Height or altitude (cm)
$\bar{\mu}$	Mean molecular weight (Da molecule^{-1})	Δ	Model layer thickness (cm)
μ_x	Molecular weight of species x (Da molecule^{-1})		
$m_{\rm H}$	Nucleon mass, 1.67×10^{-24} g	ECCM	Equilibrium cloud condensation model
P	Pressure (dyn cm^2)	AM01	Ackerman and Marley (2001)
q_c	Condensed volatile mole fraction symbol in AM01; same as D	L69	Lewis (1969)
q_s	Saturation volatile mole fraction symbol in AM01	PES	Galileo Probe entry site
q_v	Volatile (gas) mole fraction symbol in AM01; same as X	WL73	Weidenschilling and Lewis (1973)

2.2. New method: cloud density rate

Instead of directly determining cloud density, D_x, using the differential of the vapor column density, we determine a cloud density rate, R_x, using the differential of the vapor volume density. The key to accurately relating condensate density with the change in vapor density lies with the mathematical expression of the statement in WL73 that, "the difference between the partial pressure and vapor pressure is a measure of the amount of condensate which has formed in that altitude increment." But partial pressure in this model scheme is just the vapor pressure from the model layer just below, so essentially, the rate of change in saturated vapor pressure gives the rate of cloud density produced by condensation. In the next section, we explain how to convert R_x to density using an updraft parameterization.

The variation of the density of a single gaseous component x with height is

$$\frac{d\rho_x}{dz} = \frac{\mu_x}{\bar{\mu}}\left(\rho\frac{dX_x}{dz} + X_x\frac{d\rho}{dz}\right). \tag{3}$$

The first term in parentheses in Eq. (3) describes variation in the component density due to condensation. The second term varies with the change in atmospheric density with height. This term applies equally to non-condensing species, so it should be neglected when computing the change in vapor density due to condensation.

The cloud density rate is then just the complement of the change in vapor density with height:

$$R_x = -\left.\frac{d\rho_x}{dz}\right|_{\rm condensation} = -\frac{\mu_x}{\bar{\mu}}\frac{dX_x}{dz}\rho \approx \frac{\mu_x}{\bar{\mu}}\frac{X_x(I) - X_x(J)}{\Delta}\rho. \tag{4}$$

The pseudo-equality on the last line represents the simplification that the change in mole fraction with height can be approximated by the difference in mole fraction between two model layers, divided by the layer height. This is accurate as long as the model step size is small enough that dX_x/dz is roughly constant between step I and step J. This condition is met for 100-m steps in the Jupiter case, at the 1–3% level, for conditions at the three cloud bases.

We computed cloud density rates using Eq. (4), plotting them as shaded curves in Fig. 2, compared with gray lines for WL73 cloud densities. At each level z, the density and density rate obey the relation $D_x = R_x H$, as expected from the ratio of Eqs. (4) and (2). In the next subsection, we show that an updraft length scale converts the cloud density rate into a cloud density, so the factor of H in Eq. (2) represents an implicit updraft length parameter in the WL73 model.

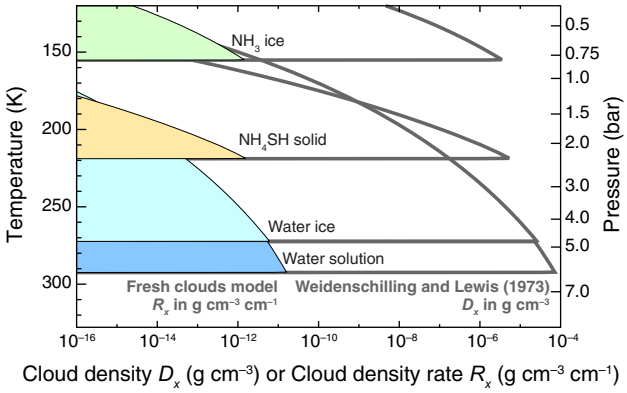

Fig. 2. Comparison of cloud density D_x, calculated using WL73's formula (our Eq. (2); gray lines), and cloud density rate R_x, using Eq. (4) (filled curves). The two curves differ dimensionally and numerically by a length factor of $H(z)$. The model assumes Galileo Probe deep mixing ratios of helium, methane, ammonia, and hydrogen sulfide (von Zahn et al., 1998; Wong et al., 2004; Mahaffy et al., 2000). Based on indirect estimates of a supersolar bulk water abundance (Wong et al., 2008), the O/H ratio was taken to be 4 times the protosolar value in Asplund et al. (2009). The temperature profiles were constrained to match Galileo Probe Atmospheric Structure Instrument and Cassini CIRS retrievals at about 400 mbar (Seiff et al., 1998; Simon-Miller et al., 2006).

2.3. Parameterized updrafts

Real clouds do not form in a perturbed closed system; the actual displaced volume depends on the duration and velocity of the updraft, and is modified by processes such as precipitation, evaporation, and advection. Within the context of the WL73 scenario, where condensed material remains at the altitude where it condenses, we can calculate first order cloud densities by scaling the cloud density rate R_x by an updraft speed and duration:

$$D_x = R_x w_* \tau_d = R_x L. \tag{5}$$

Fig. 3 graphically relates Eqs. (4) and (5). The left column shows the atmospheric state: a wet adiabatic atmosphere with saturated condensable vapor in hydrostatic equilibrium. Values here are identical to WL73. The middle column shows that the cloud density rate R_x depends on the rate of change in saturation vapor density with height. The right column shows that first-order cloud densities are produced when a column of air enters from the cloud base whose length scale (or more precisely, volume per area) can be expressed as the product of w_* and τ_d.

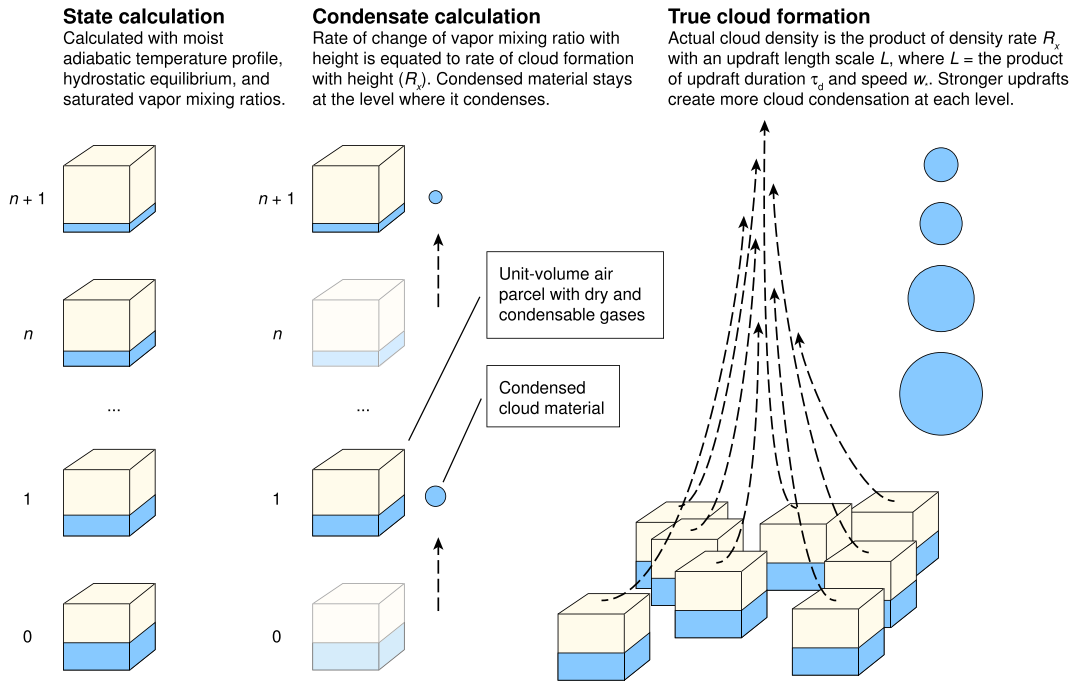

Fig. 3. Cloud density depends on updraft strength. Left column: atmospheric state is calculated at each level, describing temperature, pressure, and gas composition (same as in WL73). Middle column: the change in volatile vapor concentration with height gives the rate of cloud condensation with height (see Eq. (4)). Right column: the density rate is scaled by a characteristic length, which quantifies the mass flux, to give cloud density (see Eq. (5)). The method works for an updraft that starts and stops at any level; the same updraft strength does not need to apply over the whole atmospheric column. For an updraft with a characteristic length of one scale height, cloud densities from our model are the same as those in WL73 and are given by the gray lines in Fig. 2.

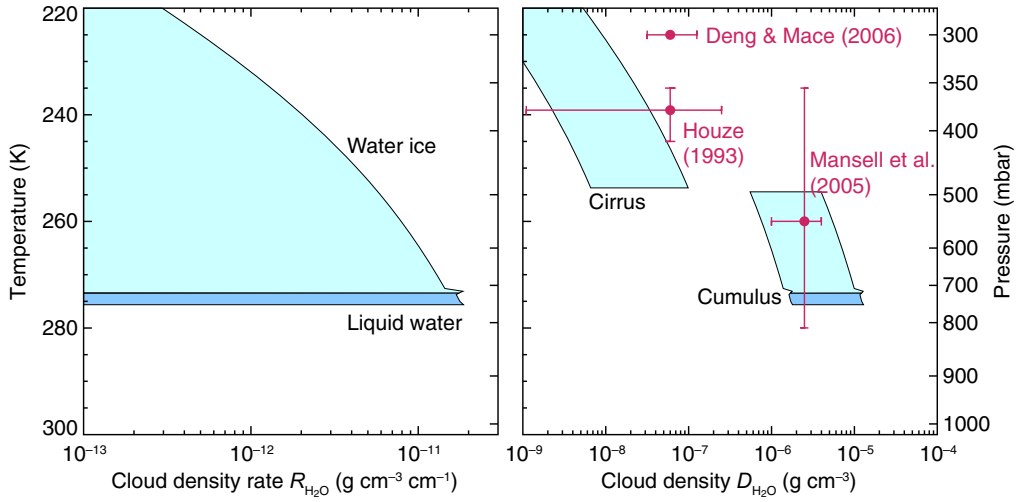

Fig. 4. Fresh cloud model density rates R_{H2O} (left) and cloud densities D_{H2O} (right) for Earth, compared with terrestrial cirrus and cumulus observations. Model initial conditions include standard atmospheric temperature and pressure (298.15 K, 1 bar), and a composition of X_{H2O} = 1% (99% dry air). The arc-shaped spread in densities at each level covers a range of updraft length scales for cirrus corresponding to updraft speeds of 0.02–0.2 m s^{-1} over a duration of 10–15 min. For cumulus, updraft speeds are 1–5 m s^{-1} for a duration of 16–23 min (Houze, 1993). Model calculations agree very well with observations of typical cirrus (Houze, 1993) and with cumulus formed in a 3D fluid model (Mansell et al., 2005). Model densities under-predict observations of a tropical anvil cirrus (Deng and Mace, 2006), partly due to neglect of transport and partly due to slower updraft velocities in the model. Vertical temperature and pressure axes are the same in both panels.

To test the accuracy of the calculation, we determine cloud densities for the atmosphere of the Earth, and compare them to the wealth of available in situ observations. In the terrestrial case, w_* and τ_d are measurable, and can be used to constrain the updraft length scale. A sample calculation, using the initial condition of X_{H2O} = 1%, yields cloud density rates and densities shown in Fig. 4.

Cirrus clouds have updraft speeds of 2–20 cm s^{-1}, with cloud condensation lasting 10–15 min (Houze, 1993, pp. 174, 188). Convective cumulus models had 1–5 m s^{-1} updrafts lasting about 20 min (Houze, 1993, pp. 260–261).

The Houze (1993) cirrus and cumulus updraft characteristics are used to determine the scaling between R_{H2O} and D_{H2O} in Fig. 4. The cloud densities calculated by this procedure agree with models and observations of both cirrus and convective cumulus clouds on Earth.

For the cirrus case, updraft length scales of 12–180 m give cloud densities of 1–100 $\times$ 10^{-9} g cm^{-3} in the 230–245 K range (Fig. 4). This encompasses the result from the Starr and Cox (1985) model with the same updraft characteristics, which calculated 30 $\times$ 10^{-9} g cm^{-3}. Observationally, cirrus cloud densities span 1–

250×10^{-9} g cm^{-3}, with 10–100×10^{-9} g cm^{-3} being most typical in the 7–8 km range (Houze, 1993, p. 174). Deng and Mace (2006) measured vertical velocities and ice water content in a tropical dissipating anvil cirrus, finding densities of about 60×10^{-9} g cm^{-3} at heights of 9–12 km. The Deng and Mace (2006) measurement exceeds model cirrus densities by about an order of magnitude. Updraft speeds of 70 cm s^{-1} in this study were larger than the typical 2–20 cm s^{-1} speeds used in our model output, accounting for some of this difference. Additionally, cloud mass transport is neglected in the fresh clouds model, but certainly important for a dissipating cirrus.

We obtain cumulus cloud base densities of 0.5–12×10^{-6} g cm^{-3}, using L = 1–7 km to describe updrafts in the 2–6 km altitude range of the atmosphere. These densities encompass the Ferrier and Houze (1989) 1-D time-dependent model result of 5×10^{-6} g cm^{-3}. A more complex 3-D model (Mansell et al., 2005) found cloud water content up to 4×10^{-6} g cm^{-3} in the 2–8 km altitude range.

Additional cumulus velocities, even when corresponding cloud densities are not available, overlap values used in our study. Both updraft speeds and durations were derived by Oktem and Romps (2013), who studied the development of convective cumulus clouds using stereo imaging sequences. They found typical updraft durations of 10 min, and velocities ranging from 3 to 16 m/s. Velocities were roughly constant over the full duration of cloud formation. Updrafts spanned vertical extents from start to end of 2–6 km. For convective cumulus, we found length scales of ~3 km, which provides a good match to updraft extents from Oktem and Romps (2013). Heymsfield et al. (2010) reviewed a decade of nadir-viewing doppler radar observations of convective clouds, made with the ER-2 research aircraft flying at altitudes of ~20 km. Many clouds in these studies were precipitating systems, so our fresh clouds model may overestimate cloud densities for these cases. Peak updraft vertical velocities in these convective systems fell in the 6–30 m s^{-1} range, and cloud particle fall speed corrections were used based on cloud densities of 10^{-6} g cm^{-3}. Kollias et al. (2001) observed velocities within fair-weather cumulus, using millimeter-wave radar sensitive to smaller non-precipitating particles. With velocities of about 6 m s^{-1} and durations on the order of a minute, our model would estimate cloud densities near 10^{-7} g cm^{-3}. This is less dense than estimates for other convective cumulus clouds, but reasonable since the fair-weather cumuli studied by Kollias et al. (2001) were relatively shallow (~700-m height).

Cloud densities derived from ECCM data using Eq. (5) are good estimates of "fresh" clouds: clouds in the early stages of formation where condensation is the dominant microphysical process. In the first 100–1000 s of cloud formation, condensation has the shortest microphysical timescale, so it has the dominant effect on cloud particle evolution (Rossow, 1978; Carlson et al., 1988). Although fresh cloud density is well modeled by adiabatic condensation in an updraft of constant velocity and finite duration, densities in mature or complex clouds depend on the effects of processes such as precipitation, evaporation, growth through coagulation and coalescence, and advection of condensate material.

The fresh clouds model calculates only cloud creation by condensation, and not the subsequent reduction of density as particles grow and precipitate out. For more evolved clouds, a different approach would be needed, such as the steady-state model of Ackerman and Marley (2001).

2.4. Ackerman and Marley (2001)

Ackerman and Marley (2001) use a different 1-D modeling approach to calculate cloud densities. The AM01 scheme parameterizes vertical transport of vapor and condensed material using eddy diffusion, with a diffusion coefficient constrained by the planetary intrinsic luminosity. In common practice today, the diffusion constant is calculated for each model layer assuming radiative–convective equilibrium (e.g., Morley et al., 2014). The condensed material rains out, with a parameterized efficiency of precipitation.

Our cloud density rate calculation, as described in Section 2.3, requires external specification of updraft time and velocity scales at every level, to convert cloud density rate to cloud density via Eq. (4). The atmospheric structure is self-consistently calculated and always moist-adiabatic in the ECCM. A non-unique combination of w_* and τ_d basically specify an updraft length scale L. In contrast, the AM01 approach allows the calculation of vertical distributions of cloud material—based on competing effects of precipitation and turbulence—but requires external specification of the atmospheric structure. In this diffusive model, eddy diffusion K and convective length scale L are specified. Both approaches, although simple, are useful for investigating atmospheric structure and cloud densities, with the fresh clouds model describing a single updraft event and cloud creation through condensation, and the diffusive model describing a steady state balance between turbulent transport and precipitation.

The master equation for condensation of cloud material in AM01 is based on L69. An actual equation is not given in L69, but the paper says that for saturated conditions, the condensable vapor mixing ratio at level J is initially equal to that at adjacent level I below, $q_v(J)|_{\text{initial}} = q_v(I) = q_s(I)$. But since $T(J) < T(I)$, $q_v(J)$ would be supersaturated. Condensation then establishes equilibrium in saturated conditions. Eq. (1) of AM01 gives the mole fraction of solid material produced via condensation:

$$q_c|_{new} = q_v|_{\text{initial}} - q_s = q_v(I) - q_s(J) = q_s(I) - q_s(J). \tag{6}$$

Weidenschilling and Lewis (1973) noted that the cloud densities in L69 depend on the model layer thickness Δ. Fig. 1 of AM01 shows output of an L69 calculation. In this case, the model step size was a little over 1 km near the cloud base (A. Ackerman, personal communication, January 2014). For the value of cloud-base q_c in the figure, we derive the same cloud densities by assuming an updraft length scale of about 100 m. However, if a model step size of 0.5 km is used instead, then q_c based on Eq. (6) is reduced by a factor of 0.4 (the steep dependence of the saturation vapor pressure on temperature means that the relationship between model step size and q_c is not linear).

However, the full AM01 model also includes turbulent transport of vapor and cloud material, in addition to condensation. The cloud density as a function of height in the AM01 diffusive/precipitative model is found by solving their Eq. (4):

$$-K\frac{dq_t}{dz} - f_{\text{rain}} w_* q_c = 0. \tag{7}$$

Using the definitions of q_t and K from AM01 and R_x from Eq. (4), we can express Eq. (7) as an inhomogeneous differential equation that is linear in q_c, with R_x as the source term:

$$L\frac{dq_c}{dz} + f_{\text{rain}} q_c - \frac{\bar{\mu}}{\mu_x \rho} L R_x = 0. \tag{8}$$

This single equation can be numerically solved to derive profiles of cloud density $q_c = D_x$ as a function of composition and height. The source term includes the condensation process, avoiding the need to iteratively approach a simultaneous solution to both Eqs. (6) and (7) as described in AM01. Qualitatively, solutions for large and small values of f_{rain} in Eq. (8) will resemble solutions shown in Fig. 1 of AM01, although an offset depending on model step size may be present due to their handling of the condensation source term.

Terms L and w_* appear in both the fresh cloud Eq. (5) as well as the AM01 evolved cloud Eqs. (7) and (8). The terms are defined dif-

ferently in each case, but serve very similar purposes. In the fresh clouds case, condensation immediately follows upward transport, and the updraft speed and length scale are w_* and L. In the evolved cloud case, there is an equilibrium between cloud material production through condensation, and loss through precipitation and evaporation. The terms w_* and L in the evolved cloud case are scales of the convective eddies that advect air upwards, again delivering volatile species for condensation.

3. Results

Cloud density data are hard to come by. In most cases, more easily obtained data like temperature profiles or cloud pressure levels are compared with 1D adiabatic models like ECCMs. Only cloud densities are affected by the approach we introduced in Sections 2.2 and 2.3. The Galileo Probe's in situ measurements of cloud densities in Jupiter's atmosphere provided a unique opportunity to apply the fresh clouds approach to study the conditions in the probe entry site.

3.1. Galileo Probe entry site

The Galileo Probe descended into a 5-μm hot spot, a feature in Jupiter's atmosphere characterized by depleted volatile gas abundances and depleted cloud opacity (Bjoraker et al., 1986; Niemann et al., 1998; Ortiz et al., 1998; Ragent et al., 1998; Atreya et al., 1999). The Probe entry site, despite its anomalous meteorology, provides a benchmark for cloud studies because it is the only location where cloud mass was measured in situ.

3.2. Comparison to ECCM

Atreya et al. (1999) used the ECCM to demonstrate that the pressure levels of cloud bases detected in the probe entry site could be matched if depleted abundances of condensable gases were used in the model (Fig. 4 of Atreya et al., 1999). Our revised condensate density formula does not alter cloud base levels, since the thermal structure determined by the model is not affected. However, Table 4 in Atreya et al. (1999) listed upper limits to column densities of jovian clouds. We use the intersection of model and observed cloud density ranges in Fig. 5 to derive updraft length scales, which are listed in Table 2 along with cloud density rates and best fit cloud column densities.

Probe site air is thought to have been deflected downwards by a planetary wave, resulting in large depletions of condensable volatiles (e.g., Showman and Ingersoll, 1998; Friedson, 2005). Given the volatile depletion in the probe entry site, and the high thermal infrared brightness in 5-μm hot spots, cloud column densities should be much lower than in other parts of Jupiter's atmosphere.

Comparison of probe site cloud column densities with "old ECCM" column densities is straightforward; model cloud densities are higher than in situ measurements by 10^3–10^7. This was recognized by Atreya et al. (1999), who suggested that the column densities may have been significantly reduced by precipitation. But the old ECCM model had an implicit updraft length scale of H, which corresponds to a very strong updraft. Since vigorous updrafts should be rare in 5-μm hot spots, the old ECCM model was driven to over-predict cloud densities.

Comparison of probe site cloud column densities with "fresh clouds model" column density rates requires an extra step: scaling by $w_*\tau_d$ (or equivalently by L) to convert column density rate to column density. Fig. 5 demonstrates this process: for a given cloud, a range of column densities can be derived (slanted lines) depending on the chosen value of L. Offsets between the lines for each modeled cloud layer correspond to differences in cloud composition and in the ranges of pressures considered for each cloud layer. Values of L were selected based on this figure, and then listed for each cloud layer in Table 2. To be compatible with widescale downwelling in the probe site, one might expect the updraft length scale L to be rather small, and characteristic of weak localized turbulence rather than a strong upwelling.

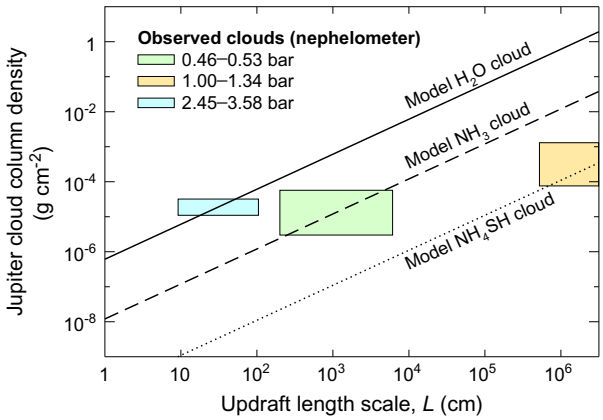

Fig. 5. Comparison between observed clouds in the Galileo Probe entry site and modeled fresh clouds. Observed cloud column densities (vertical extents of the shaded boxes) are based on nephelometer measurements integrated over the given pressure ranges (Ragent et al., 1998). Model cloud column densities for each cloud composition are given by the slanted lines, as a function of updraft length scale L. Model cloud column densities are calculated for the same pressure ranges as the observed clouds; column density rate is the value of each line as it crosses $L = 1$ cm. Updraft length scales thus correspond to the intersections of the lines and boxes.

4. Discussion

4.1. Probe entry site updrafts

Due to the long radiative timescale in Jupiter's atmosphere, only updrafts are likely to be able to provide the rapid cooling necessary to create cloud material through condensation. The fact that clouds (albeit thin clouds) were detected in the probe entry site implies that at least localized updrafts were present, despite evidence that 5-μm hot spots are generally characterized by downward advection.

In Section 2.3, we used model R_x and observed terrestrial updraft characteristics to calculate cloud density, which we compared with observed terrestrial cloud densities. But in the probe entry site, we instead determine how strong an updraft is needed to produce the observed cloud densities, based on model cloud density rates.

Table 2 lists cloud column densities σ_x and column density rates σ_x rate. These quantities are vertically integrated analogs of D_x and R_x, respectively, because the proportionality factor between σ_x and σ_x rate is also L. We use model σ_x rate and σ_x from nephelometer retrievals to solve for L, constraining dynamic conditions in the PES. The best comparison can be made using the column labeled "PES height" for the new model, which includes cloud material integrated only over the same restricted pressure ranges where clouds were retrieved based on nephelometer data. A consistent story is told by the lower and upper clouds, while the middle cloud has an anomalously high density.

The deepest cloud is considered a "water" cloud because it was found at depths where NH_3 and NH_4SH would be subsaturated (based on their deep abundances as measured by the probe well below the cloud layers). For this cloud, Table 2 indicates that σ_{NH3} rate differs from the observed σ_{NH3} by a length scale of around 20–60 cm. Following Eq. (5), this means the observed cloud is consistent with a very weak updraft. An updraft length scale of

Table 2
Probe entry site (PES) cloud column densities: observations[a] vs. models.[b]

	Galileo Probe nephelometer (PES)	Old ECCM (PES height)	Fresh clouds model (PES height)	Old ECCM (full height)	Fresh clouds model (full height)
Water cloud properties					
P (bar)	2.45–3.58	2.45–3.58	2.45–3.58	5.96	5.96
T_{base} (K)	247	250	250	292	292
σ_{H2O} (g cm^{-2})	$1.1–3.2 \times 10^{-5}$[a]	2.4[c]	2.4×10^{-5}[c]	61.8[c]	2.4×10^{-5}[c]
σ_{H2O} rate (g cm^{-2} cm^{-1})	–	–	6.1×10^{-7}	–	1.4×10^{-5}
$L = w_* \tau_d$ (cm)[d]	–	–	40	–	1.7
NH_4SH cloud properties					
P (bar)	1.0–1.34	1.0–1.34	1.0–1.34	2.32	2.32
T_{base} (K)	176	185	185	219	219
σ_{NH4SH} (g cm^{-2})	$7.6–130 \times 10^{-5}$[a]	3.2×10^{-4}[c]	11×10^{-5}[c]	1.56[c]	11×10^{-5}[c]
σ_{NH4SH} rate (g cm^{-2} cm^{-1})	–	–	1.1×10^{-10}	–	4.5×10^{-7}
$L = w_* \tau_d$ (cm)[d]	–	–	10^6	–	240
NH_3 cloud properties					
P (bar)	0.46–0.53	0.46–0.53	0.46–0.53	0.78	0.78
T_{base} (K)	138	136	136	155	155
σ_{NH3} (g cm^{-2})	$0.3–5.7 \times 10^{-5}$[a]	2.6×10^{-2}[c]	1.2×10^{-5}[c]	1.13[c]	3×10^{-5}[c]
σ_{NH3} rate (g cm^{-2} cm^{-1})	–	–	1.2×10^{-8}	–	4.7×10^{-7}
$L = w_* \tau_d$ (cm)[d]	–	–	1000	–	64

[a] Nephelometer σ is retrieved in situ cloud mass loading (Table 3 in Ragent et al., 1998).
[b] Model calculations are shown in Fig. 2. "Old ECCM" calculations use the WL73 method for calculating cloud density (Section 2.1), and "fresh clouds" calculations use the parameterized updraft method (Section 2.2).
[c] Model cloud column densities are calculated by Eqs. (2) and (5) for old ECCM and fresh clouds models respectively, after integrating over the same vertical extent as the PES clouds ("PES height" columns), or over the full vertical extent of the equilibrium cloud ("full height" columns).
[d] New "fresh clouds" model column densities depend on the choice of updraft length scale L, a tunable free parameter. Values of L given in the table were selected to provide a good match to the probe column density measurements.

20–60 cm corresponds for example to a duration of 20 s and a speed of 1–3 cm s^{-1}. Updraft speed and duration are fully degenerate, but any combination of these parameters consistent with a 40-cm updraft length scale would match the observations.

A similar exercise for the NH_3 cloud shows that at least a 10 times higher updraft length scale is needed, e.g., with at least a speed of 12 cm s^{-1} for the same 20-s duration as found for the water cloud. An updraft length scale of 250–4800 cm for this NH_3 cloud is consistent with updraft characteristics of a terrestrial cirrus cloud. So the NH_3 cloud is still quite thin, and qualitatively consistent with large-scale downwelling over the region surrounding the Galileo Probe entry site, perhaps with fresh cirrus formed by localized weak turbulence within the downdraft.

The middle cloud retrieved from probe nephelometer data is not so simply interpreted. In this region near $T = 180$ K, the air should be clearer of condensed cloud material than at other levels within the cloud layers (Fig. 2). The saturation vapor pressures of water and H_2S over NH_4SH are very small, and it is too warm still for NH_3 to condense. At this level of just over 1 bar pressure, water may contribute more cloud material than NH_4SH, although neither species should have particularly high condensate density here, compared to other altitudes closer to the equilibrium cloud bases. We label the cloud NH_4SH, but its composition is poorly constrained observationally and theoretically, compared to the water and ammonia clouds. In fact, it has been suggested that $(NH_4)_2S$ may condense instead of NH_4SH (Lewis and Prinn, 1970; Ibragimov and Solodovnik, 1991; Atreya et al., 1999).

Solving for L in Eq. (5) implies a strong updraft in order to scale the very small σ_{NH4SH} rate by a length scale factor of $\sim 10^6$ cm to match the observed σ_{NH4SH}. This could be achieved by an updraft speed of 10 m s^{-1} over a duration of 1000 s, similar to the updraft characteristics of a terrestrial convective cumulus cloud. A slightly weaker (by maybe a factor of 10) updraft could be consistent with the observations, if both water and NH_4SH cloud material were considered to comprise the observed cloud. Although cumulus-type convective motions may be needed, the resulting cloud density is still much smaller than that in a cumulus cloud, because the 1-bar region is so far from the cloud bases of NH_4SH and water.

A vigorous updraft near the 1-bar level, similar to terrestrial convective cumulus, may not be very consistent with what is known about 5-μm hot spots like the one entered by the Galileo Probe. Generally subsiding motion is thought to be responsible for the very volatile-depleted and essentially cloud-free conditions that allow 5-μm infrared radiation to escape from the 4-bar level or deeper (e.g., Bjoraker et al., 1986). If localized turbulence could create updraft fluxes consistent with a 1000-s updraft near 1 bar—where saturation vapor pressures are so low that very little cloud matter would condense to trace these motions—then similar cumulus-type updrafts would be expected to be found at other levels as well. This would produce thick observable clouds at other levels, at odds with observations of clear, dry hot spots.

Uncertainties in the composition of the middle nephelometer cloud layer may explain the inconsistency between the model updraft characteristics for this cloud, and the weak updrafts required for the water and ammonia clouds. A different cloud composition, with an equilibrium cloud base located closer to the observed cloud level at $T \sim 180$ K, would have greater R_x and permit the density of the middle cloud layer to be better explained in terms of a weaker updraft. Adsorption of NH_3 onto ices in this region could also increase the mass of condensed material (de Pater et al., 2001). These effects would bring the required updraft strengths more in line with 5-μm hot spot dynamics. A comprehensive modern laboratory campaign to explore the actual composition of condensed material in the NH_3–H_2S system near 200 K would be able to investigate this possibility.

Volatile gas mixing ratios, measured by the Galileo Probe Mass Spectrometer, may also provide clues that there is a non-NH_4SH cloud sink for H_2S. In the column-stretching description of 5-μm hot spots (Showman and Ingersoll, 1998), volatile mixing ratio profiles are vertically distorted by the passage of an equatorially-trapped wave. To first order, a probe entry site equilibration level—the level where a volatile mixing ratio reaches its deep

value—is a fossilized signature of a cloud base in the un-stretched column.

The relative abundances of NH_3:H_2S:H_2O at the probe entry site equilibration levels differ by orders of magnitude from the relative abundances at cloud base levels in equilibrium models (Wong et al., 2004). In particular, at the probe site NH_3 equilibration level, the H_2S mixing ratio was found to be about 10^6 larger than at the NH_3 cloud base in the equilibrium case, corresponding to an un-stretched saturated column. This very large discrepancy may be due to dynamical effects, since actual volatile mixing ratios are controlled by vertical transport, horizontal mixing, and transport/vaporization of cloud material, in addition to condensation. But it is difficult to invoke dynamics to explain the NH_3:H_2S ratios in this case, without an additional mechanism to segregate the two condensable gases.

Alternately, the NH_3:H_2S ratio at the NH_3 equilibration level may indicate that H_2S condenses as another compound in Jupiter's atmosphere. To increase X_{H2S} by 10^6 times (compared to its value at the NH_3 cloud base), the sulfur-containing cloud base would need to move upward by about 1 bar to $P < 1.5$ bar. This would seem to contradict a number of radiative transfer retrievals suggesting a widespread cloud layer at 2 bar in Jupiter's atmosphere (West et al., 2004, and references therein).

4.2. Jupiter cloud densities in other models

Several recent time-dependent models provide benchmarks for comparison with the cloud densities from our parameterized updraft model. There is general consistency between cloud densities in our 1-D static fresh cloud model, and cloud densities in models with more complex dynamics. This validates our method, which although simpler, is nonetheless valuable in that it can estimate fresh cloud densities for a range of specific updraft situations, from weak cirrus-forming updrafts to stronger and more sustained cumulus-forming updrafts.

Palotai and Dowling (2008) implemented a full microphysical treatment of cloud formation and evolution within a three-dimensional fluid model. The models produced updraft speeds of 6–14 cm s^{-1}. Typical cloud densities in their equatorial convective simulation were 10^{-7} g cm^{-3} for the water cloud and 6.5×10^{-8} g cm^{-3} for the ammonia cloud. Using our Eq. (5), these cloud densities and updraft speeds correspond to updraft durations of 10–30 min for the water cloud or 1–3 h for the ammonia cloud, for the fresh cloud case.

However, updrafts in the Palotai and Dowling (2008) model continue for tens to hundreds of days, appropriate for more evolved clouds. The sedimentation timescale, based on model output max sedimentation velocities of 4 m s^{-1} for NH_3 and 20 m s^{-1} for liquid H_2O, is 2000–5000 s. These sedimentation timescales are in the 0.5–1.5 h range, spanning the range of updraft durations from our fresh clouds model required to match cloud densities in the convective model. It appears then that cloud densities in Palotai and Dowling (2008) represent a steady state between condensation and precipitation, in which the condensation timescale is equal to the precipitation timescale.

Zuchowski et al. (2009) presented an adaptation of a 3-D GCM (the OPUS model), including cloud particle evolution, which provides vertical velocity numbers that can be used with our Eq. (5) to relate ECCM cloud density rates to actual cloud densities. The authors limited their consideration of particles to small ones with sedimentation velocities of 0.1 cm s^{-1} or less, in order to ensure that precipitation was too weak to significantly deplete cloud densities. This agrees qualitatively with our conclusion above that 4–20 m s^{-1} fall speeds for precipitating particles in Palotai and Dowling (2008) enable sedimentation to balance cloud creation, achieving steady-state cloud densities in agreement between our results and Palotai and Dowling (2008).

Fig. 3 in Zuchowski et al. (2009) gives maximum horizontal mean cloud densities of 2–4 $\times$ 10^{-9} g cm^{-3} for the NH_3 and NH_4SH clouds, and 10^{-7} g cm^{-3} for the water cloud. They also give a characteristic vertical velocity of +0.3 cm s^{-1}. Combining these values in Eq. (5), updraft durations required to produce the Zuchowski et al. (2009) cloud densities are about 2 h for the NH_3 cloud and 9 h for the H_2O cloud. For the ammonia cloud, this is a similar updraft duration to what we found matches Palotai and Dowling (2008) cloud densities, but the much smaller vertical velocity in Zuchowski et al. (2009) results in an ammonia cloud with an order of magnitude lower cloud density. Water cloud densities are similar in both 3-D models, but Eq. (5) demonstrates that these densities can either be created in tens of minutes for stronger updrafts as in Palotai and Dowling (2008), or in about one jovian day for the weaker mean updraft in Zuchowski et al. (2009).

Sugiyama et al. (2011) presented a 2-D fluid model, with full production and loss of clouds of H_2O, NH_4SH, and NH_3; and the results are compared with an ECCM implementation. The main conclusions of this paper relied on the output of the 2-D fluid model, in which cloud densities are controlled by dynamics. Densities as high as 10^{-7} g cm^{-3} are found in convective events with velocities of 10 m s^{-1}. According to Eq. (5), these conditions would require an updraft lasting 1000 s, which is similar to updraft durations for terrestrial cumulus clouds.

In summary, cloud densities in terrestrial models and observations, as well as in time-dependent fluid models of Jupiter's atmosphere (Palotai and Dowling, 2008; Sugiyama et al., 2011; and Zuchowski et al., 2009), are consistent with cloud densities from our fresh clouds parameterized updraft model, when updraft length scale is well constrained.

Our revision to the method of WL73 for calculating densities of clouds in the atmosphere of Jupiter does not change the lapse rate or the equilibrium cloud condensation level. Cloud densities from the model can span orders of magnitude, depending on the updraft length scale. Interpretation of certain data, such as microwave emissions from Jupiter (Janssen et al., 2005) might depend on cloud density. The greatest effect would result from a strong updraft in the case where the water abundance in Jupiter's well-mixed atmosphere is significantly greater than solar, producing a thick liquid water cloud.

5. Conclusions

One-dimensional equilibrium cloud models are still valuable tools for planetary and exoplanetary research, as evidenced from the ongoing rate of citations to fundamental papers such as WL73 and AM01. For equilibrium condensation models, calculation of cloud densities has been challenging. By combining cloud density rates from the ECCM with a parameterized updraft, first-order cloud densities can be calculated.

Dynamically, cloud densities depend on the advection of vapor, as well as microphysical processes affecting the creation, growth, and loss of particles. Ackerman and Marley (2001) addressed the dynamical aspect of cloud formation by parameterizing advection and precipitation in terms of turbulent diffusion and a precipitation efficiency f_{rain}. This was an advance over the absence of dynamical and microphysical processes in basic ECCMs like WL73. The scheme of combining ECCM output with a parameterized updraft is another advance. Our parameterized updraft model, and the diffusive/precipitative model of AM01, are complementary 1D schemes. Our fresh clouds model simulates direct cloud formation through condensation, with vapor delivered via an organized updraft. The AM01 model simulates a steady-state cloud in balance

between a condensation source via diffusive convection and precipitative loss; this is an evolved cloud scenario.

We validated our parameterized updraft method of cloud density calculation by comparing with terrestrial cloud densities, for both a convective cumulus and a cirrus case. These cases were distinguished by different formation levels and updraft characteristics. The WL73 ECCM would be unable to model both types of clouds, since it cannot distinguish between the two different vapor flux cases.

We also show that clouds in the Galileo Probe entry site, as measured by the nephelometer, are consistent with weak updrafts of limited duration. This finding is well aligned with our dynamical understanding of the probe entry site as a region of widescale downwelling, where intense or sustained updrafts would not have been expected to be present (e.g., Friedson, 2005). This interpretation of the probe cloud measurements is much simpler than that invoked in prior works such as Atreya et al. (1999), where ECCM cloud densities were too high, requiring precipitative loss processes to be invoked in every case. Of course microphysical processes such as coagulation, coalescence, evaporation, disruption, and precipitation are significant in all clouds in addition to condensation. Our fresh clouds model is most appropriate to young clouds in the formative process, where condensation is the dominant microphysical effect.

For the middle cloud discovered by the Galileo Probe nephelometer, at about the 1-bar level, our method can match cloud densities of water and NH_4SH only if strong cumulus-type updrafts are present. Strong updrafts are generally not expected within 5-μm hot spots, and specifically contradict the much smaller updraft length scales and cirrus-type updrafts derived for the upper and lower cloud layers in the probe entry site. Strong updrafts are also inconsistent with models and remote sensing observations of 5-μm hot spots, where large-scale downwelling is thought to be responsible for the depleted cloud opacity and volatile mixing ratios. The cloud densities in the middle layer observed by the probe nephelometer therefore provide a suggestion that perhaps cloud density rates are increased by the condensation of an alternate (non-NH_4SH) sulfur–nitrogen compound, or by ammonia adsorption onto other ices in this temperature range.

Acknowledgments

Andrew Ingersoll brought to our attention non-conservation of mass in prior ECCM implementations. We thank Andy Ingersoll and Steve Levin for improving the elegance of our expressions, and Rick Smith and Rusen Oktem for additional helpful discussions. Andy Ackerman and Mark Marley provided substantial assistance in comparison with their model. This work was supported in part by Juno subcontract 699056KC to SKA from SwRI, and by NASA under Grant No. NNX11AM55G to MHW issued through the Outer Planets Research program.

References

Ackerman, A.S., Marley, M.S., 2001. Precipitating condensation clouds in substellar atmospheres. Astrophys. J. 556, 872–884.
Asplund, M., Grevesse, N., Sauval, A.J., Scott, P., 2009. The chemical composition of the Sun. Annu. Rev. Astron. Astrophys. 47, 481–522.
Atreya, S.K. et al., 1999. A comparison of the atmospheres of Jupiter and Saturn: Deep atmospheric composition, cloud structure, vertical mixing, and origin. Planet. Space Sci. 47, 1243–1262.
Bjoraker, G.L., Larson, H.P., Kunde, V.G., 1986. The abundance and distribution of water vapor in Jupiter's atmosphere. Astrophys. J. 311, 1058–1072.
Carlson, B.E., Rossow, W.B., Orton, G.S., 1988. Cloud microphysics of the giant planets. J. Atmos. Sci. 45, 2066–2081.
Deng, M., Mace, G.G., 2006. Cirrus microphysical properties and air motion statistics using cloud radar doppler moments. Part I: Algorithm description. J. Appl. Meteorol. Climatol. 45, 1690–1709.
de Pater, I., Dunn, D., Romani, P., Zahnle, K., 2001. Reconciling Galileo Probe data and ground-based radio observations of ammonia on Jupiter. Icarus 149, 66–78.
Ferrier, B.S., Houze Jr., R.A., 1989. One-dimensional time-dependent modeling of GATE cumulonimbus convection. J. Atmos. Sci. 46, 330–352.
Friedson, A.J., 2005. Water, ammonia, and H_2S mixing ratios in Jupiter's 5-μm hot spots: A dynamical model. Icarus 177, 1–17.
Heymsfield, G.M., Tian, L., Heymsfield, A.J., Li, L., Guimond, S., 2010. Characteristics of deep tropical and subtropical convection from nadir-viewing high-altitude airborne doppler radar. J. Atmos. Sci. 67, 285–308.
Houze, R.A., 1993. Cloud Dynamics. Academic Press, San Diego CA.
Ibragimov, K.Y., Solodovnik, A.A., 1991. Ammonium hydrosulfide and clouds in the atmospheres of the giant planets. Kinematics Phys. Celest. Bodies 7, 53–58.
Janssen, M.A., Hofstadter, M.D., Gulkis, S., Ingersoll, A.P., Allison, M., Bolton, S.J., Levin, S.M., Kamp, L.W., 2005. Microwave remote sensing of Jupiter's atmosphere from an orbiting spacecraft. Icarus 173, 447–453.
Kollias, P., Albrecht, B.A., Lhermitte, R., Savtchenko, A., 2001. Radar observations of updrafts, downdrafts, and turbulence in fair-weather cumuli. J. Atmos. Sci. 58, 1750–1766.
Lewis, J.S., 1969. The clouds of Jupiter and the NH_3–H_2O and NH_3–H_2S systems. Icarus 10, 365–378.
Lewis, J.S., 1995. Physics and Chemistry of the Solar System. Academic Press, San Diego CA.
Lewis, J.S., Prinn, R.G., 1970. Jupiter's clouds: Structure and composition. Science 169, 472–473.
Mahaffy, P.R. et al., 2000. Noble gas abundance and isotope ratios in the atmosphere of Jupiter from the Galileo Probe Mass Spectrometer. J. Geophys. Res. 105, 15061–15072.
Mansell, E.R., Macgorman, D.R., Ziegler, C.L., Straka, J.M., 2005. Charge structure and lightning sensitivity in a simulated multicell thunderstorm. J. Geophys. Res.: Atmos. 110. Article id: D12101.
Morley, C.V. et al., 2014. Water clouds in Y dwarfs and exoplanets. Astrophys. J. Article id: 78.
Niemann, H.B. et al., 1998. The composition of the jovian atmosphere as determined by the Galileo Probe Mass Spectrometer. J. Geophys. Res. 103, 22831–22846.
Oktem, R., Romps, D.M., 2013. Observing vertical motion of deep convective clouds by stereo photogrammetry. American Geophysical Union (Fall) Meeting, Abstract A11E-0096.
Ortiz, J.L., Orton, G.S., Friedson, A.J., Stewart, S.T., Fisher, B.M., Spencer, J.R., 1998. Evolution and persistence of 5-μm hot spots at the Galileo Probe entry latitude. J. Geophys. Res. 103, 23051–23069.
Palotai, C., Dowling, T.E., 2008. Addition of water and ammonia cloud microphysics to the EPIC model. Icarus 194, 303–326.
Ragent, B. et al., 1998. The clouds of Jupiter: Results of the Galileo Jupiter mission probe nephelometer experiment. J. Geophys. Res. 103, 22891–22910.
Rossow, W.B., 1978. Cloud microphysics—Analysis of the clouds of Earth, Venus, Mars, and Jupiter. Icarus 36, 1–50.
Seiff, A. et al., 1998. Thermal structure of Jupiter's atmosphere near the edge of a 5-μm hot spot in the north equatorial belt. J. Geophys. Res. 103, 22857–22890.
Showman, A.P., Ingersoll, A.P., 1998. Interpretation of Galileo Probe data and implications for Jupiter's dry downdrafts. Icarus 132, 205–220.
Simon-Miller, A.A., Conrath, B.J., Gierasch, P.J., Orton, G.S., Achterberg, R.K., Flasar, F.M., Fisher, B.M., 2006. Jupiter's atmospheric temperatures: From Voyager IRIS to Cassini CIRS. Icarus 180, 98–112.
Starr, D.O., Cox, S.K., 1985. Cirrus clouds. Part II: Numerical experiments on the formation and maintenance of cirrus. J. Atmos. Sci. 42, 2682–2694.
Sugiyama, K. et al., 2011. Intermittent cumulonimbus activity breaking the three-layer cloud structure of Jupiter. Geophys. Res. Lett. 38. Article id: L13201.
von Zahn, U., Hunten, D.M., Lehmacher, G., 1998. Helium in Jupiter's atmosphere: Results from the Galileo Probe helium interferometer experiment. J. Geophys. Res. 103, 22815–22830.
Weidenschilling, S.J., Lewis, J.S., 1973. Atmospheric and cloud structures of the jovian planets. Icarus 20, 465–476.
West, R.A., Baines, K.H., Friedson, A.J., Banfield, D., Ragent, B., Taylor, F.W., 2004. Jovian clouds and haze. In: Bagenal, F., Dowling, T.E., McKinnon, W.B. (Eds.), Jupiter. Cambridge Univ. Press, Cambridge, pp. 79–104.
Wong, M.H., Mahaffy, P.R., Atreya, S.K., Niemann, H.B., Owen, T.C., 2004. Updated Galileo Probe Mass Spectrometer measurements of carbon, oxygen, nitrogen, and sulfur on Jupiter. Icarus 171, 153–170.
Wong, M.H. et al., 2008. Oxygen and other volatiles in the giant planets and their satellites. In: MacPherson, G.J., Mittlefehldt, D.W., Jones, J., Simon, S.B. (Eds.), Oxygen in the Solar System, Reviews in Mineralogy and Geochemistry, vol. 68. Mineralogical Society of America, Chantilly, VA, pp. 219–246.
Zuchowski, L.C., Yamazaki, Y.H., Read, P.L., 2009. Modeling Jupiter's cloud bands and decks. 2. Distribution and motion of condensates. Icarus 200, 563–573.